

# The Optical Gravitational Lensing Experiment. Period–Luminosity Relations of Variable Red Giant Stars\*

I. Soszyński<sup>1</sup>, W.A. Dziembowski<sup>1</sup>, A. Udalski<sup>1</sup>,  
M. Kubiak<sup>1</sup>, M.K. Szymański<sup>1</sup>, G. Pietrzyński<sup>1,2</sup>,  
Ł. Wyrzykowski<sup>1,3</sup>, O. Szewczyk<sup>1,2</sup>, and K. Ulaczyk<sup>1</sup>

<sup>1</sup>Warsaw University Observatory, Al. Ujazdowskie 4, 00-478 Warszawa, Poland  
e-mail:

(soszynsk,w,d,udalski,mk,msz,pietrzyn,wyrzykow,szewczyk,kulaczyk)@astrouw.edu.pl

<sup>2</sup> Universidad de Concepción, Departamento de Física, Casilla 160–C,  
Concepción, Chile

<sup>3</sup> Institute of Astronomy, University of Cambridge, Madingley Road,  
Cambridge CB3 0HA, UK

## ABSTRACT

Period–luminosity (PL) relations of variable red giants in the Large (LMC) and Small Magellanic Clouds (SMC) are presented. The PL diagrams are plotted in three planes:  $\log P$ – $K_S$ ,  $\log P$ – $W_{JK}$ , and  $\log P$ – $W_I$ , where  $W_{JK}$  and  $W_I$  are reddening free Wesenheit indices. Fourteen PL sequences are distinguishable, and some of them consist of three closely spaced ridges. Each of the sequences is fitted with a linear or quadratic function. The similarities and differences between the PL relations in both galaxies are discussed for four types of red giant variability: OGLE Small Amplitude Red Giants (OSARGs), Miras and Semiregular Variables (SRVs), Long Secondary Periods (LSPs) and ellipsoidal variables.

We propose a new method of separating OSARGs from non-variable stars and SRVs. The method employs the position in the reddening-free PL diagrams and the characteristic period ratios of these multiperiodic variables. The PL relations for the LMC OSARG are compared with the calculated relations for RGB models along isochrones of relevant ages and metallicities. We also compare measured periods and amplitudes of the OSARGs with predictions based on the relations valid for less luminous solar-like pulsators.

Miras and SRVs seem to follow PL relation of the same slopes in the LMC and SMC, while for LSP and ellipsoidal variables slopes in both galaxies are different. The PL sequences defined by LSP variables and binary systems overlap in the whole range of analyzed wavebands. We put forward new arguments for the binary star scenario as an explanation of the LSP variability and elaborate on it further. The measured pulsation to orbital period ratio implies nearly constant ratio of the star radius to orbital distance,  $R/A \approx 0.4$ , as we find. Combined effect of tidal friction and mass loss enhanced by the low-mass companion may explain why such a value is preferred.

*Stars: AGB and post-AGB – Stars: late-type – Stars: oscillations – Magellanic Clouds*

---

\*Based on observations obtained with the 1.3-m Warsaw telescope at the Las Campanas Observatory of the Carnegie Institution of Washington.

## 1. Introduction

The first attempt to determine period–luminosity ( $PL$ ) relation for long period variables (LPVs) was made by Gerasimovič (1928), who noticed that Mira stars with longer periods are on average fainter at visual wavelengths. This result has been confirmed by subsequent studies (*e.g.*, Wilson and Merrill 1942, Osvalds and Risley 1961, Clayton and Feast 1969), however the scatter of this period–luminosity dependence turned out to be very large.

First tight  $PL$  relation for LPVs was discovered for Mira stars at near infrared (NIR) wavebands (Glass and Lloyd Evans 1981). This  $PL$  law, based on only 11 Miras in the LMC, was refined by extensive studies of Feast *et al.* (1989) and Hughes and Wood (1990). The second, parallel  $PL$  sequence, occupied by semiregular variables (SRVs), was identified by Wood and Sebo (1996). This sequence was shifted relative to the Miras’ ridge toward shorter periods by a factor of two.

However, the subject of  $PL$  distribution of LPVs has progressed rapidly over recent years when large microlensing surveys (MACHO, OGLE, EROS, MOA) published long-term photometry of huge number of stars. Complex structure of the  $PL$  distribution was demonstrated for the first time by Cook *et al.* (1997), who published  $PL$  diagram for variable stars detected during the MACHO survey in the LMC. A series of three or four  $PL$  sequences defined by LPVs can be distinguished in that diagram.

Sharper picture was presented by Wood *et al.* (1999), who distinguished and described five  $PL$  sequences (denoted as A–E) in the period–Wesenheit index plane. Wood (2000) showed similar distribution in the  $\log P$ – $K$  diagram. These results were then confirmed by many studies based on observations originated in various sources (Cioni *et al.* 2001, 2003, Noda *et al.* 2002, Lebzelter *et al.* 2002, Ita *et al.* 2004, Groenewegen 2004, Fraser *et al.* 2005).

Kiss and Bedding (2003, 2004) used OGLE data to reveal new features in the  $PL$  distribution. They noticed that sequence B consists of two closely spaced parallel ridges (Ita *et al.* 2004 denoted the additional sequence as C’). Below the tip of the red giant branch (TRGB) Kiss and Bedding (2003) found three sequences shifted in  $\log P$  relative to stars brighter than TRGB. It was the definitive proof that stars in the first ascent Red Giant Branch (RGB) pulsate similarly to objects being in the Asymptotic Giant Branch (AGB) phase.

The Optical Gravitational Lensing Experiment (OGLE) collected unprecedented amount of photometric data of stars in the Large and Small Magellanic Clouds. Both galaxies have been constantly monitored since 1997 and at present time this is the best and longest available photometric dataset for analyzing huge number of variable red giants. Our studies on LPVs resulted in many discoveries, regarding also the  $PL$  relations.

Soszyński *et al.* (2004a) showed that OGLE Small Amplitude Red Giants (OSARGs) constitute separate class of variable stars, with different structure in the  $PL$  plane than “classical” SRVs and Miras. We indicated two previously overlooked  $PL$  relations – the longest ( $a_1$ ) and the shortest ( $a_4$ ) period sequences followed by AGB OSARGs. We also suggested a method of empirical division

between RGB and AGB OSARGs fainter than TRGB.

Red giants revealing ellipsoidal modulation caused by binarity were analyzed by Soszyński *et al.* (2004b). It was shown that, if true orbital periods are considered, the  $PL$  relation of ellipsoidal variables (sequence E) is a direct continuation of sequence D occupied by mysterious Long Secondary Period (LSP) variables. This is a hint that the LSP phenomenon may be related to binarity, but taking into account available radial velocity measurements, the secondary component usually must be a low mass object, possibly former planet. This idea was supported by Soszyński (2007) who discovered in some LSP variables ellipsoidal-like and eclipsing-like modulations with periods equal to LSPs.

In Soszyński *et al.* (2005) we again increased complexity of the PL distribution of LPVs. Each of the NIR  $PL$  sequences  $C'$ , C and D in the LMC (occupied by SRV, Miras and LSP variables) split into two separate ridges in the period – optical Wesenheit index plane, what corresponds to the spectral division into oxygen-rich (O-rich) and carbon-rich (C-rich) AGB stars. Thus, we found a new photometric method of distinguishing between these two populations.

In this paper we describe in details the  $PL$  relations of variable red giants in both Magellanic Clouds. We show new details in the  $PL$  plane and compare  $PL$  distribution in the LMC and SMC. The paper is organized as follows. Section 2 gives details of the observations and data reduction. In Section 3 the  $PL$  relations are presented with a description of their derivation. A discussion about four types of red giant variability – OSARGs, Miras/SRVs, LSPs and ellipsoidal modulation – is given in Sections 4–7. Section 8 summarizes and concludes the paper.

## 2. Observations and Data Reduction

Our analysis is based on the photometry of stars in the LMC and SMC observed during the second and third phases of the OGLE survey (OGLE-II and OGLE-III). Both galaxies have been monitored since 1997 with the 1.3-m Warsaw telescope at the Las Campanas Observatory, Chile, which is operated by the Carnegie Institution of Washington. During the OGLE-II survey (1997–2000) the telescope was equipped with the “first generation” camera with the SITE  $2048 \times 2048$  CCD detector. Details of the instrumentation setup can be found in Udalski *et al.* (1997). In 2001 the telescope equipment was upgraded to a wide field  $8192 \times 8192$  mosaic camera consisting of eight SITE CCD detectors (Udalski 2003).

In this work we used OGLE-II observations supplemented by the OGLE-III data. The OGLE-II fields cover about 4.5 square degrees in the central regions of the LMC and 2.4 square degrees in the SMC. The last observations used in this analysis were collected in February 2007, so our photometry spans 10 years. The data have been obtained in two standard  $I$  and  $V$  filters, but majority of the observations (typically 700–900 points per star) were carried out in the former bandpass. Saturation occurred for stars brighter than  $I = 12.5$  mag. In the  $V$ -band we collected about 50 points per star.

The data were reduced using the standard OGLE pipeline, as described by Udalski (2003). For details about the transformation of the instrumental photometry to the standard system and the determination of the equatorial coordinates of stars the reader is referred to Udalski *et al.* (2000). The well calibrated OGLE-II photometry and OGLE-III observations were tied using magnitudes of several dozen constant stars in the closest neighborhood around each object.

The  $K_S$  and  $J$  NIR photometry used in this analysis was taken from 2MASS All-Sky Catalog of Point Sources (Cutri *et al.* 2003). We performed cross-identification between OGLE and 2MASS sources with 1 arcsec search radius, but earlier small shifts to RA and DEC had been added to compensate for systematic differences between both coordinate systems. We found confident 2MASS counterparts for 98% of red stars observed by OGLE. For further analysis, we included only stars with all four  $-V$ ,  $I$ ,  $J$  and  $K_S$  bands available.

### 3. Period–Luminosity Relations for Variable Red Giants

A period analysis for all stars with  $(V - I) > 0.5$  mag and  $I < 17$  mag (in the SMC with  $I < 17.5$  mag) was performed with program FNPEAKS developed by Z. Kołaczowski (private communication). The frequency range searched was from 0.0 to 0.9 cycles per day. For each light curve we determined the highest peak in the Fourier spectrum, then the third order Fourier series was fitted to the observations and subtracted from it. The procedure was repeated on the residual data until fifteen periods per star were derived. Moreover, we recorded the amplitudes and signal-to-noise (S/N) parameters associated with each period.

We constructed  $PL$  diagrams in three variants for both galaxies:  $\log P - K_S$ ,  $\log P - W_{JK}$ , and  $\log P - W_I$ .  $K_S$  is the 2MASS single epoch magnitude with no compensation applied for interstellar reddening. The single epoch random phase observations cause additional spread in the  $PL$  relations for large amplitude variables. This effect has been avoided for Miras and SRVs thanks to converting single epoch observations into mean magnitudes using complete  $I$ -band light curves. Details of this method were described by Soszyński *et al.* (2005).

$W_{JK}$  and  $W_I$  are NIR and optical Wesenheit indices (Madore 1982), *i.e.*, reddening free quantities being a linear combinations of selected magnitudes and colors:

$$W_{JK} = K_S - 0.686(J - K_S) \quad (1)$$

$$W_I = I - 1.55(V - I) \quad (2)$$

The  $PL$  diagrams for LMC and SMC are shown in Fig. 1 and Fig. 3, respectively. We present here only the stars that have been used to determine the  $PL$  relations. For Miras and SRVs, LSP and ellipsoidal variables only one point per star is shown, while for OSARGs more periods per star may be displayed. Detailed description of the criteria used for the selection of variables are given in the next four Sections. The LMC  $PL$  sequences appear better defined which may be explained by much larger sample of objects and by much smaller depth in the line of sight of the LMC than the SMC.

To derive possibly most precise regression lines we first converted the  $PL$  diagrams into density maps and found points along the given  $PL$  sequence where the density of points is the largest. Then, we performed linear or quadratic least square fit to these points. Note that the described method produces regression functions in general different than ordinary least square fits to the  $PL$  points, *i.e.*, we usually obtained steeper lines. Figs. 2 and 4 shows the functions fitted to the  $PL$  sequences. The same functions are given in Tables 1 and 2.

At  $K_S$  and  $W_{JK}$  the  $PL$  relations have been approximated by linear functions, while  $\log P-W_I$  laws have usually been fitted with quadratic functions, because of distinct curvature of these relations. This non-linearity is associated curvature of the distribution visible in the color-magnitude  $(V-I)-I$  diagram. Optical and NIR color-magnitude diagrams for stars included in Figs. 1 and 3 are shown in Fig. 5. One can notice different features of  $(V-I)-I$  and  $(J-K)-K$  distributions in both Clouds. Note, that the coefficients of the parabolas fitted to the period- $W_I$  relations (Tables 1 and 2) have considerable errors. Nevertheless, one may find these coefficients useful.

In the next Sections we describe in more details four classes of variable red giants visible in the  $PL$  diagrams.

## 4. OGLE Small Amplitude Red Giants

The name ‘‘OGLE Small Amplitude Red Giants’’ (OSARGs) has been proposed by Wray *et al.* (2004), who analyzed about 18 000 of such objects in the Galactic bulge using OGLE-II photometry. The term ‘‘OSARG’’ is not fully synonymous with ‘‘Small Amplitude Red Variable’’ (SARV) from the classification introduced by Eggen (1977, and references within), *i.e.*, stars with visual amplitudes smaller than 0.5 mag. As shown by Soszyński *et al.* (2004a) the OSARG variables cannot be distinguished from ‘‘classical’’ SRVs (hereafter just SRVs) using solely amplitudes of variations, because this is an overlapping property of both groups. Moreover, Eggen’s SARVs include wide variety of stellar types, while OSARG variables constitute a separate class of variable stars (Soszyński *et al.* 2004a).

It is known that all red giants of type K5 and cooler are variable in brightness, and amplitude of variations increases with decreasing temperature of the stars (Edmonds and Gilliland 1996, Henry *et al.* 2000). Using OGLE photometry we can detect stars with  $I$ -band peak-to-peak amplitudes as small as 4 mmag.

Table 1  
Period–Luminosity Relations of LPVs in the LMC

| Sequence          |        | $K_S = \alpha(\log P - 2.0) + \beta$ |                  | $W_{JK} = \alpha(\log P - 2.0) + \beta$ |                  | $W_I = \alpha \log^2 P + \beta \log P + \gamma$ |         |          |         |
|-------------------|--------|--------------------------------------|------------------|---|------------------|---|---------|----------|---------|
|                   |        | $\alpha$                             | $\beta$          | $\alpha$                                | $\beta$          | $\alpha$  | $\beta$ | $\gamma$ |         |
| OSARGs            | RGB    | b <sub>1</sub>                       | $-3.34 \pm 0.04$ | $11.51 \pm 0.02$                        | $-3.81 \pm 0.05$ | $10.64 \pm 0.02$                                | -2.648  | 3.780    | 13.098  |
|                   |        | b <sub>2</sub>                       | $-3.58 \pm 0.04$ | $10.94 \pm 0.02$                        | $-3.96 \pm 0.04$ | $10.03 \pm 0.03$                                | -3.396  | 5.118    | 12.182  |
|                   |        | b <sub>3</sub>                       | $-3.72 \pm 0.05$ | $10.22 \pm 0.03$                        | $-4.02 \pm 0.05$ | $9.32 \pm 0.02$                                 | -3.564  | 4.473    | 12.592  |
|                   | AGB    | a <sub>1</sub>                       | $-3.69 \pm 0.04$ | $11.13 \pm 0.02$                        | $-3.92 \pm 0.04$ | $10.31 \pm 0.02$                                | -1.604  | 0.254    | 15.782  |
|                   |        | a <sub>2</sub>                       | $-3.70 \pm 0.03$ | $10.59 \pm 0.02$                        | $-3.99 \pm 0.03$ | $9.70 \pm 0.02$                                 | -1.669  | -0.106   | 15.731  |
|                   |        | a <sub>3</sub>                       | $-3.80 \pm 0.04$ | $9.98 \pm 0.03$                         | $-4.04 \pm 0.04$ | $9.08 \pm 0.03$                                 | -1.556  | -0.905   | 15.878  |
|                   |        | a <sub>4</sub>                       | $-4.01 \pm 0.04$ | $9.40 \pm 0.04$                         | $-4.18 \pm 0.04$ | $8.51 \pm 0.04$                                 | -1.382  | -1.839   | 16.235  |
| Miras<br>and SRVs | O-rich | C <sub>O</sub>                       | $-4.17 \pm 0.08$ | $12.59 \pm 0.04$                        | $-4.34 \pm 0.09$ | $11.84 \pm 0.04$                                | -9.803  | 33.672   | -16.149 |
|                   |        | C' <sub>O</sub>                      | $-4.35 \pm 0.07$ | $11.25 \pm 0.02$                        | $-4.67 \pm 0.07$ | $10.39 \pm 0.02$                                | -9.169  | 25.589   | -5.158  |
|                   | C-rich | C <sub>C</sub>                       | $-4.07 \pm 0.11$ | $12.71 \pm 0.06$                        | $-5.19 \pm 0.11$ | $12.01 \pm 0.06$                                | -6.618  | 25.468   | -12.522 |
|                   |        | C' <sub>C</sub>                      | $-4.06 \pm 0.08$ | $11.39 \pm 0.04$                        | $-4.89 \pm 0.08$ | $10.39 \pm 0.04$                                | -3.133  | 7.278    | 8.830   |
| LSPs              | O-rich | D <sub>O</sub>                       | $-4.41 \pm 0.07$ | $15.05 \pm 0.05$                        | $-4.64 \pm 0.08$ | $14.43 \pm 0.05$                                | -5.882  | 23.707   | -10.128 |
|                   | C-rich | D <sub>C</sub>                       | $-4.38 \pm 0.25$ | $15.26 \pm 0.23$                        | $-5.09 \pm 0.28$ | $14.92 \pm 0.26$                                | 0.0     | -7.71    | 33.44   |
| Ell.              | E      | $-3.41 \pm 0.10$                     | $14.48 \pm 0.06$ | $-3.79 \pm 0.11$                        | $13.92 \pm 0.06$ | 0.0   | -3.94   | 22.20    |         |

Table 2  
Period–Luminosity Relations of LPVs in the SMC

| Sequence          |        | $K_S = \alpha(\log P - 2.0) + \beta$ |                  | $W_{JK} = \alpha(\log P - 2.0) + \beta$ |                  | $W_I = \alpha \log^2 P + \beta \log P + \gamma$ |         |          |        |
|-------------------|--------|--------------------------------------|------------------|---|------------------|---|---------|----------|--------|
|                   |        | $\alpha$                             | $\beta$          | $\alpha$                                | $\beta$          | $\alpha$  | $\beta$ | $\gamma$ |        |
| OSARGs            | RGB    | b <sub>1</sub>                       | $-3.56 \pm 0.07$ | $11.83 \pm 0.04$                        | $-3.84 \pm 0.08$ | $11.05 \pm 0.04$                                | -1.448  | 0.655    | 15.482 |
|                   |        | b <sub>2</sub>                       | $-3.88 \pm 0.07$ | $11.21 \pm 0.04$                        | $-4.25 \pm 0.08$ | $10.33 \pm 0.04$                                | -2.844  | 4.134    | 12.874 |
|                   |        | b <sub>3</sub>                       | $-4.40 \pm 0.07$ | $10.14 \pm 0.05$                        | $-4.48 \pm 0.09$ | $9.39 \pm 0.05$                                 | -3.583  | 4.782    | 12.639 |
|                   | AGB    | a <sub>1</sub>                       | $-3.66 \pm 0.04$ | $11.55 \pm 0.02$                        | $-4.02 \pm 0.05$ | $10.74 \pm 0.03$                                | -0.520  | -2.574   | 18.041 |
|                   |        | a <sub>2</sub>                       | $-3.89 \pm 0.04$ | $10.85 \pm 0.02$                        | $-4.11 \pm 0.04$ | $10.06 \pm 0.03$                                | -1.111  | -0.912   | 16.248 |
|                   |        | a <sub>3</sub>                       | $-4.04 \pm 0.05$ | $10.19 \pm 0.04$                        | $-4.40 \pm 0.05$ | $9.25 \pm 0.04$                                 | -1.179  | -1.090   | 16.001 |
|                   |        | a <sub>4</sub>                       | $-4.29 \pm 0.04$ | $9.52 \pm 0.03$                         | $-4.49 \pm 0.04$ | $8.89 \pm 0.04$                                 | -0.688  | -2.886   | 16.997 |
| Miras<br>and SRVs | O-rich | C <sub>O</sub>                       | $-4.14 \pm 0.17$ | $12.90 \pm 0.05$                        | $-4.39 \pm 0.19$ | $12.14 \pm 0.05$                                | -6.900  | 23.341   | -6.495 |
|                   |        | C' <sub>O</sub>                      | $-4.47 \pm 0.15$ | $11.62 \pm 0.03$                        | $-4.94 \pm 0.15$ | $10.81 \pm 0.03$                                | -3.816  | 8.379    | 9.106  |
|                   | C-rich | C <sub>C</sub>                       | $-4.22 \pm 0.16$ | $13.11 \pm 0.07$                        | $-5.26 \pm 0.14$ | $12.43 \pm 0.06$                                | -3.991  | 12.486   | 3.605  |
|                   |        | C' <sub>C</sub>                      | $-4.40 \pm 0.15$ | $11.88 \pm 0.04$                        | $-5.05 \pm 0.13$ | $10.90 \pm 0.04$                                | -3.482  | 7.933    | 9.362  |
| LSPs              | O-rich | D <sub>O</sub>                       | $-4.13 \pm 0.11$ | $15.16 \pm 0.08$                        | $-4.40 \pm 0.11$ | $14.61 \pm 0.08$                                | -4.752  | 19.487   | -6.363 |
|                   | C-rich | D <sub>C</sub>                       | $-4.11 \pm 0.30$ | $15.39 \pm 0.30$                        | $-4.46 \pm 0.33$ | $14.77 \pm 0.30$                                | 0.0     | -7.00    | 31.40  |
| Ell.              | E      | $-3.15 \pm 0.12$                     | $14.70 \pm 0.07$ | $-3.32 \pm 0.16$                        | $14.10 \pm 0.07$ | 0.0   | -3.90   | 22.43    |        |

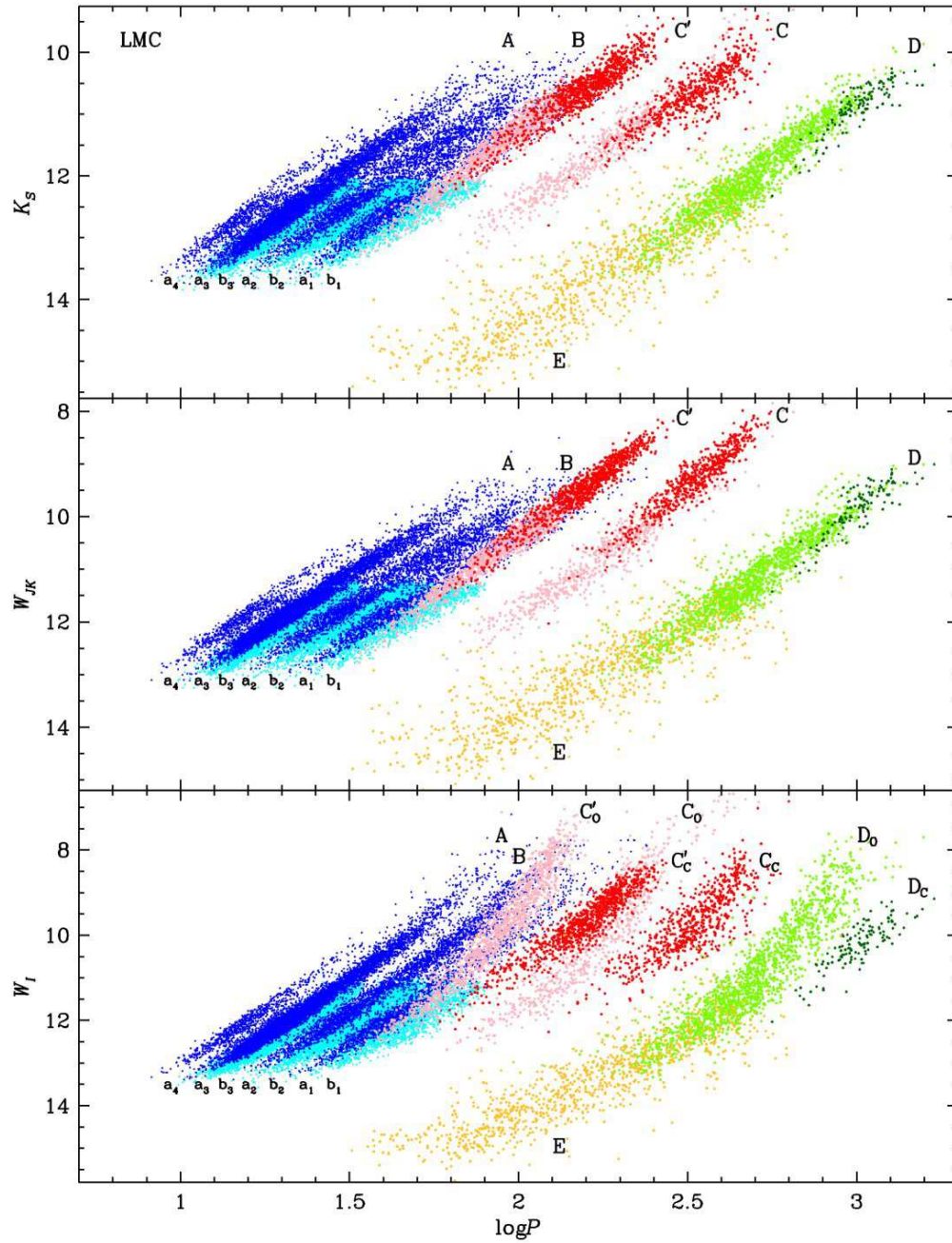


Fig. 1. Period–luminosity diagrams of variable red giants in the LMC. OSARG variables are shown as blue points (RGB as light blue, AGB as dark blue). Miras and SRVs are marked with pink (O-rich) and red (C-rich) points. Light and dark green points refer to O-rich and C-rich LSP variables, respectively. Yellow points indicate ellipsoidal red giants.

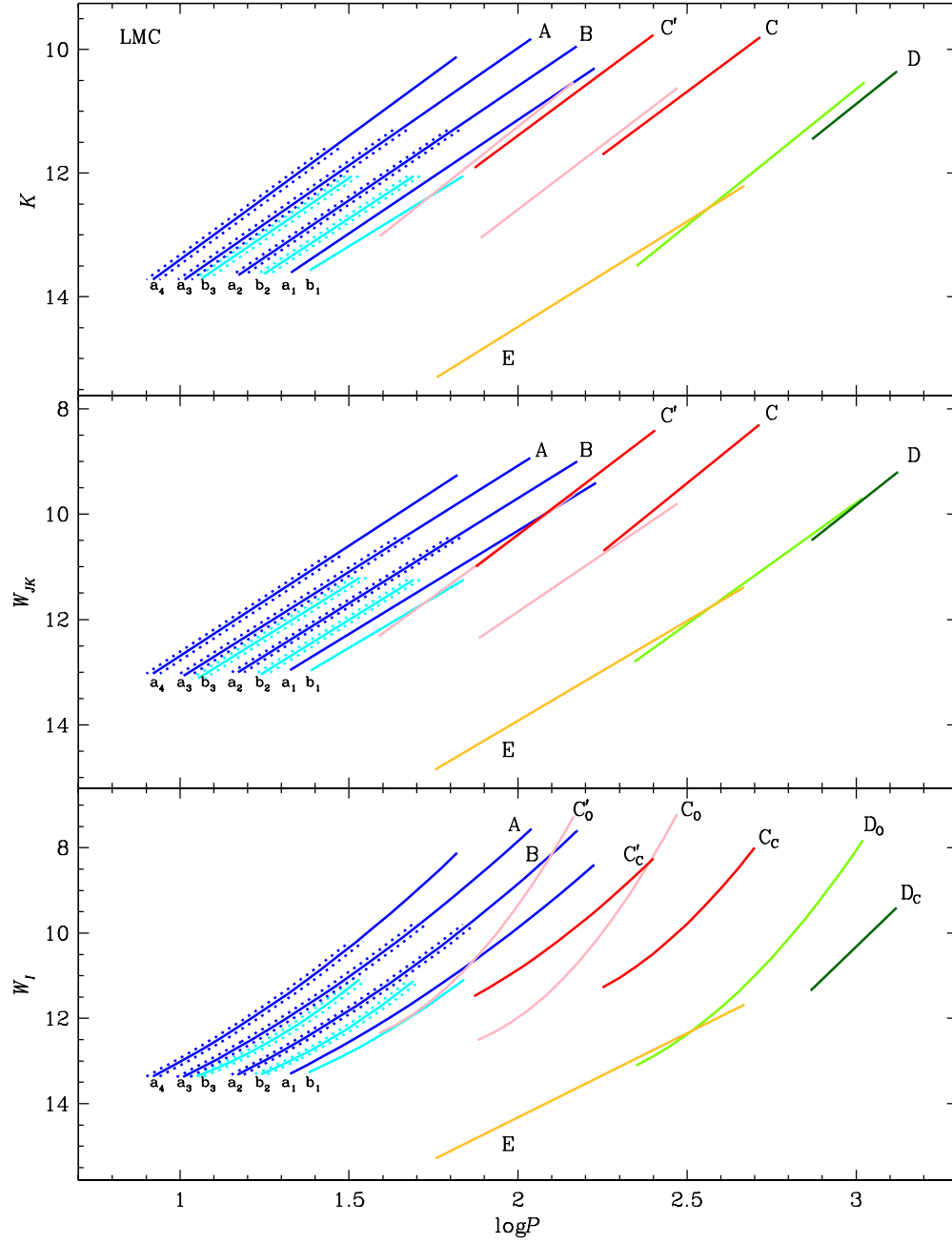


Fig. 2. Period–luminosity relations for red giants in the LMC fitted to the sequences shown in Fig. 1. The colors of lines indicate the same types of stars as in Fig. 1.



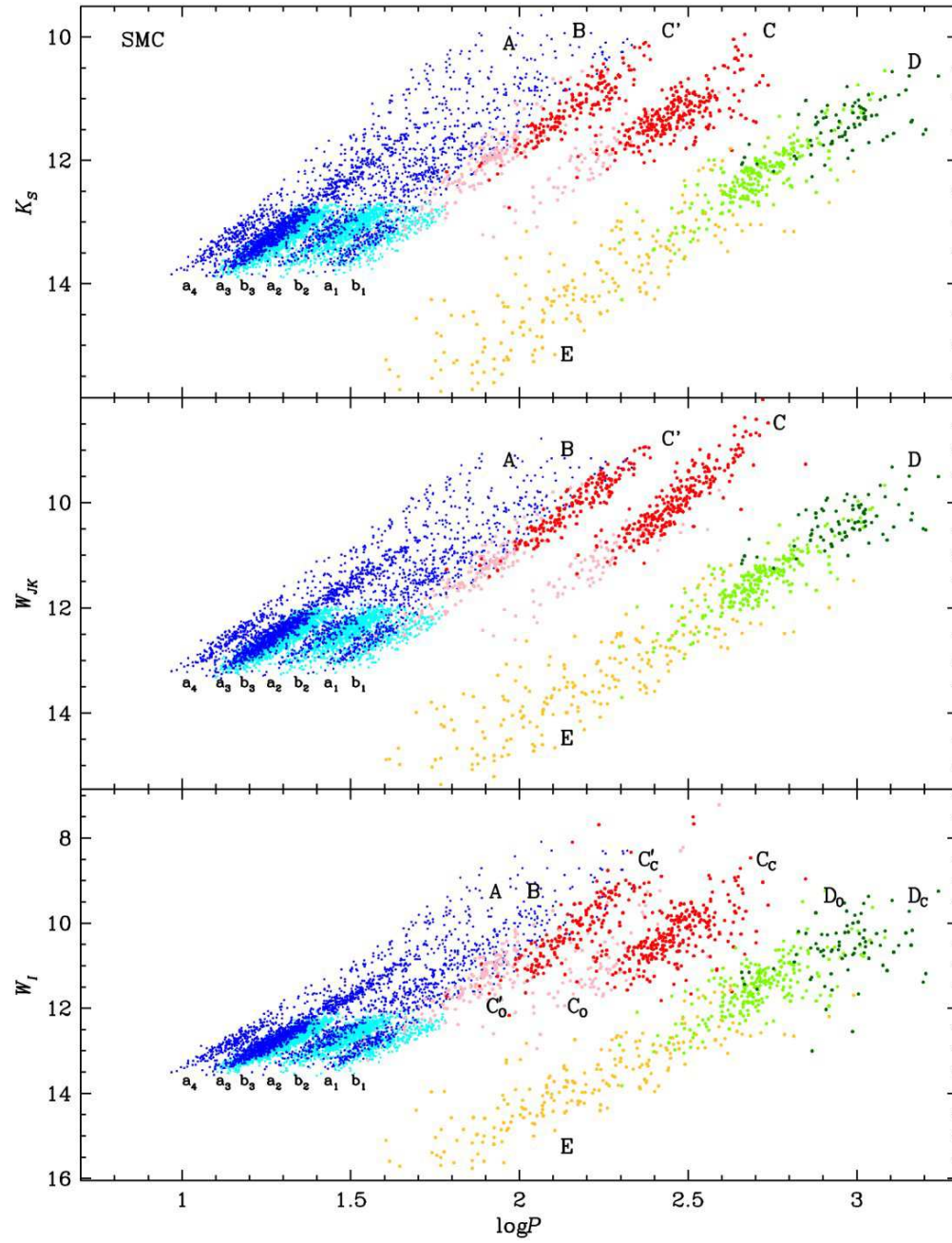


Fig. 3. Period–luminosity diagrams of variable red giants in the SMC. The colors represent the same types of stars as in Fig. 1.

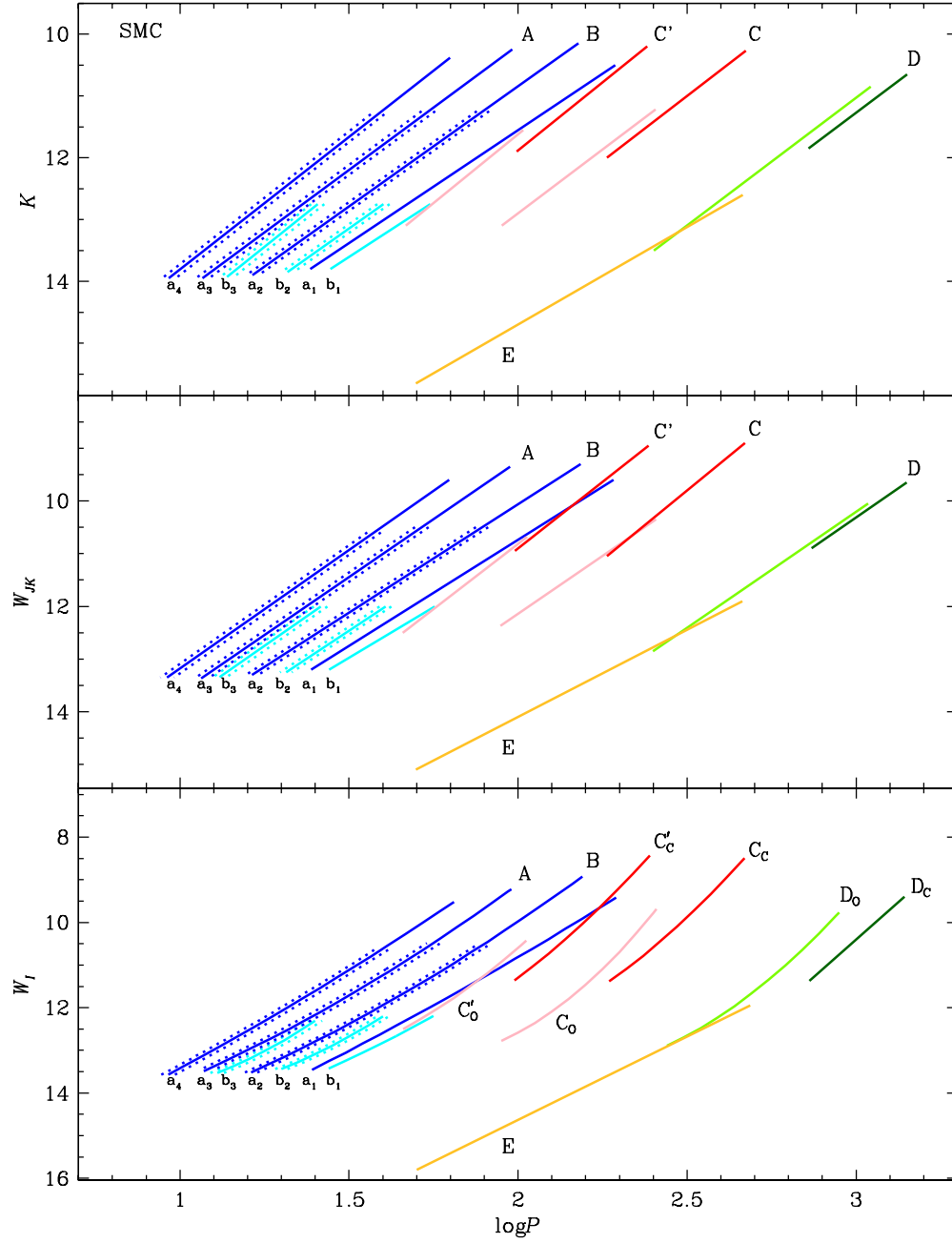


Fig. 4. Period–luminosity relations for red giants in the SMC fitted to the sequences shown in Fig. 3. The colors of lines indicate the same types of stars as in Fig. 1.

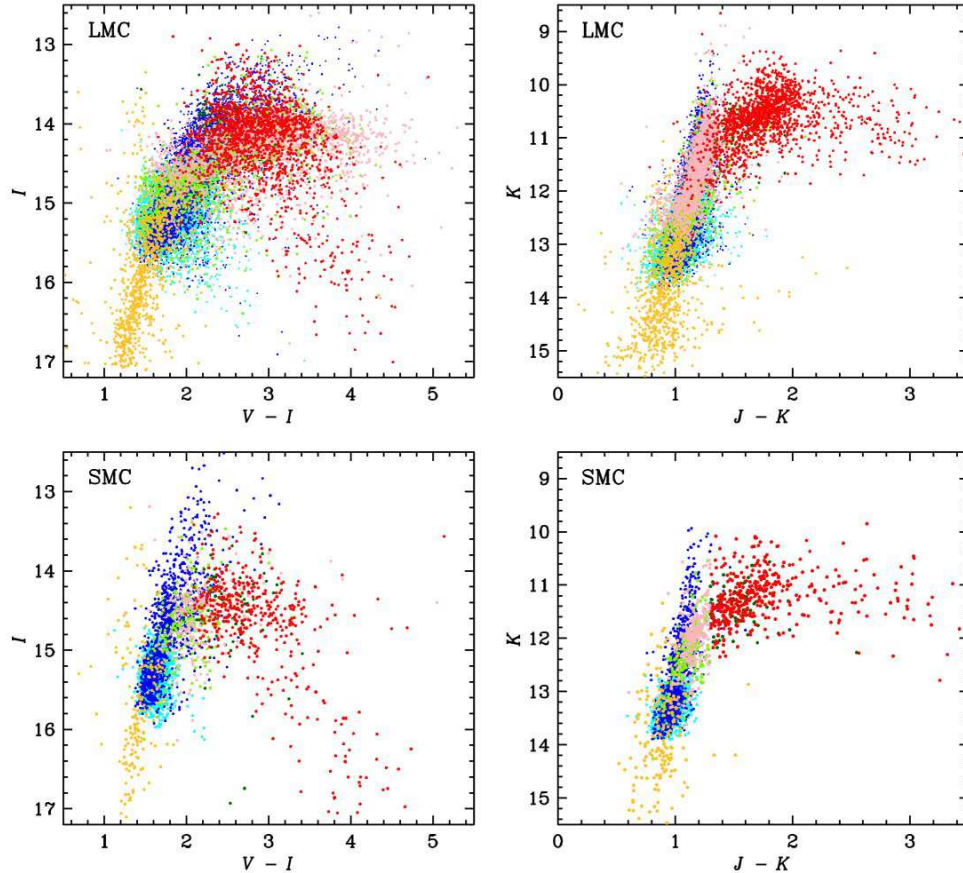


Fig. 5. Color–magnitude diagrams for LMC (*upper panels*) and SMC (*lower panels*) variable red giants. The colors represent the same types of stars as in Fig. 1.

#### 4.1 Selection of OSARGs

Since OSARGs with the smallest detectable amplitudes are mixed with constant stars (strictly speaking, with stars having amplitudes too small to be visible in our data), it is not an easy task to separate both groups. Likewise, the longest period sequences of OSARGs overlap with *PL* ridge of SRVs, thus a separation of the two populations is in general problematic. Any of simple diagrams that can be prepared using available parameters of stars (periods, magnitudes, colors, amplitudes) did not enable us to precisely separate long-period OSARGs from SRVs, and faintest OSARGs from non-variable stars.

To solve this problem we worked out a new method of OSARG variables detection. Our algorithm takes into account a star position on the PL diagrams

and characteristic period ratios of these multiperiodic variables. Our basic tool is the diagram  $\Delta \log P_L - P_S/P_L$ , where  $P_S$  and  $P_L$  is any pair of periods (shorter and longer, respectively) selected from the most significant periodicities of the given star, and  $\Delta \log P_L$  is a horizontal distance of  $\log P_L$  from selected sequence in the selected  $PL$  plane (in our analysis from sequence A).

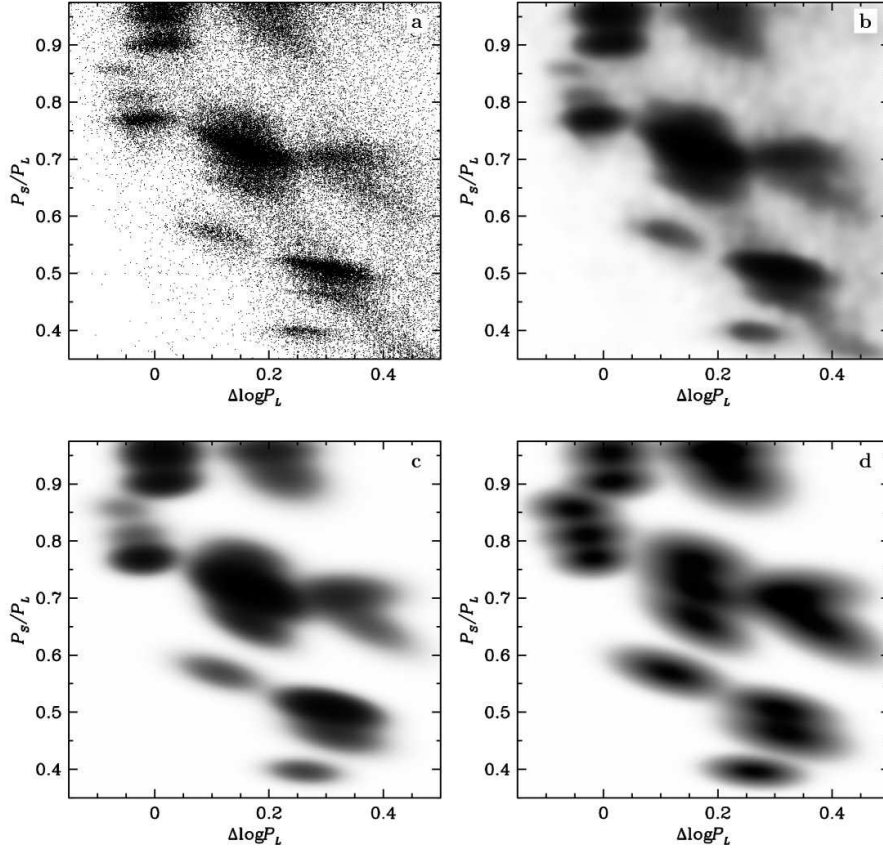


Fig. 6. Diagram  $\Delta \log P_L - P_S/P_L$  for OSARG variables in the LMC.  $P_S$  and  $P_L$  are, respectively, any shorter and longer periods of a given star.  $\Delta \log P_L$  is a horizontal distance from sequence A in  $\log P - W_I$  plane. See text for detailed description.

Fig. 6a shows such a diagram for OSARGs tentatively selected from our data.  $\Delta \log P_L$  in this diagram were measured in the  $\log P_L - W_I$  plane, but very similar picture was independently obtained using  $\log P_L - W_{JK}$  diagram. Distinct groups of points are fingerprints of the OSARG variability. In order to utilize this distribution for selecting OSARGs, we smoothed it with a Gaussian filter and derived density map visualized in Fig. 6b.

Then, we fitted two-dimensional Gauss function to every group of points visible in Fig. 6b, and prepared artificial density map which is shown in Fig. 6c.

In this way we rejected points which occurred in the  $\Delta \log P_L - P_S/P_L$  diagrams by chance from spuriously detected periods. The last step of our procedure was normalization of our map, *i.e.*, setting up the maxima of all fitted Gaussian at the same level (Fig. 6d). Thanks to that every pair of periods was treated with the same weight, regardless of which  $PL$  relations corresponded to these periods. Two such maps as shown in Fig. 6d have been prepared – one with  $\Delta \log P_L$  measured in the  $\log P_L - W_I$  plane, and the second in the  $\log P_L - W_{JK}$  diagram.

The procedure of selecting OSARG variables was performed as follows. For each star we examined each pair of periods (selected from 15 derived periods) for which S/N parameter was larger than 3.0. We derived ratios of both periods and  $\Delta \log P_L$  parameters in the  $\log P_L - W_I$  and  $\log P_L - W_{JK}$  planes. Then, for subsequent Gaussians shown in Fig. 6d we calculated values in respective ( $\Delta \log P_L, P_S/P_L$ ) points, thus only points close to the maximum of the given Gaussian produced values significantly larger than zero. Additionally, we took the product of the values obtained with the two Wesenheit indices so that the values for accidental points were close to zero.

We co-added every such derived value for each Gaussian and each pair of periods. Resulting sum is an indicator of the OSARG variability. For the best candidates for OSARG variables this quantity is larger than 10. For our purposes we set the threshold of the OSARG indicator to be larger than 3. Our method allows effective discrimination of OSARGs from non-variable stars, as well as from SRVs.

## 4.2 Period–Luminosity Relations for OSARGs

The OSARGs constitute probably the most numerous class of variable stars in the Magellanic Clouds. We selected about 17000 such objects in the LMC and about 3500 in the SMC, which is more than a number of Cepheids, RR Lyr stars, eclipsing binaries and other types of variable red giants. OSARG variables brighter than TRGB ( $K_S = 12.05$  mag in the LMC,  $K_S = 12.7$  mag in the SMC) were obviously recognized as AGB stars, while below TRGB we separated RGB and AGB stars using the feature noticed by Soszyński *et al.* (2004a). If any of the periods falls on the shortest-period sequence  $a_4$ , the star was recognized as AGB object. Otherwise we marked the OSARG as RGB star, although small contribution of AGB may still exist among these group. In Figs. 1–5 RGB OSARGs are marked with light blue points and lines, while AGB OSARGs are drawn in dark blue.

As shown by Soszyński *et al.* (2004a) OSARGs follow a series of three (RGB stars) or four (AGB stars) narrow sequences, spreading over periods ranging from 8 to 160 days. In this paper we use labels introduced by Soszyński *et al.* (2004a):  $a_1 - a_4$  for AGB and  $b_1 - b_3$  for RGB OSARGs. The  $PL$  relations of RGB OSARGs are shifted in  $\log P$  relative to AGB OSARGs, what can be explained by the temperature difference of both populations at the same luminosity (Kiss and Bedding 2003). Soszyński *et al.* (2004a) also showed that the third sequence (*i.e.*, sequences  $a_3$  and  $b_3$  or Wood’s sequence A) is split into three ridges, what manifests itself in the period – period ratio diagram with

distinct groups of points around  $P_S/P_L \approx 0.9$  and  $P_S/P_L \approx 0.95$ . We marked these two additional  $PL$  relations with dotted lines in Figs. 2 and 4. We observe this feature for RGB and AGB stars located below the TRGB and for some AGB objects brighter than the TRGB. For the brightest stars this split is not visible in our data.

Our new analysis revealed that the same feature may also concern other  $PL$  sequences of OSARG variables. Similar clouds for period ratios 0.9 and 0.95 are clearly visible for the second sequence ( $a_2$  and  $b_2$ ). For the fourth sequence ( $a_4$ ) this property is marginally visible, what can be an effect of smaller number of stars that follow this shortest period relation. Nevertheless, we also drew the additional dotted lines in the  $PL$  diagrams for this ridge. For the first, longest period sequences ( $a_1$  and  $b_1$ ) we cannot detect any distinct group of points close to the period ratio 0.9 or 0.95.

It seems that  $PL$  sequences for OSARG variables are best separated in the  $\log P - W_I$  diagram. This plane also reveals the largest differences between red giants in the LMC and SMC. The  $PL$  sequences in the LMC are significantly steeper and are more curved than those in the SMC. This difference may be directly related to different distribution of points in the color–magnitude ( $V - I$ ,  $V$ ) diagrams given in Fig. 5, what may reflect differences in ages and metallicity of red giants between the SMC and LMC. In both galaxies, the slopes of the OSARG  $PL$  relations increase with decreasing periods.

It is natural to associate the  $PL$  sequences with individual modes of stellar oscillations. Identification of the modes would yield new constraints on models of red giants as well as on star formation in the Magellanic Clouds. As an illustration, we considered the  $b_1$ ,  $b_2$ , and  $b_3$  sequences in the LMC, assuming that they correspond to first three radial modes.

Salaris and Girardi (2005) showed that the upper part of the RGB in the LMC is composed of stars with heavy element abundance in the wide range, from  $[\text{Fe}/\text{H}] = -1$  to  $-0.3$ , which corresponds to age between 1 and 11 Gy. However, for most of the objects  $[\text{Fe}/\text{H}] = -0.65 \pm 0.1$  and there is a gap in star formation between 7 Gy and 9 Gy.

Our theoretical  $PL$  relations were based on the BaSTI (Pietrinferni *et al.* 2004) isochrones. For each model, we recalculated envelope structure and determined the radial mode periods. The  $W_I$  index was calculated from  $V$  and  $I$  data from BaSTI assuming 18.45 mag for the distance modulus. A comparison of the selected theoretical and observed sequences is shown in Fig. 7. Note that fitting requires younger and more metal abundant objects at higher luminosities. The agreement between observed and calculated relations, though not perfect seems encouraging. Detailed comparison requires simulation of the the LMC RGB population. The result will certainly differ somewhat from simulation based in the CMD data presented in Fig. 5 of Salaris and Girardi (2005) and reconciling the results will require new modeling. It is likely that the four  $a_k$  sequences correspond to first four radial modes.

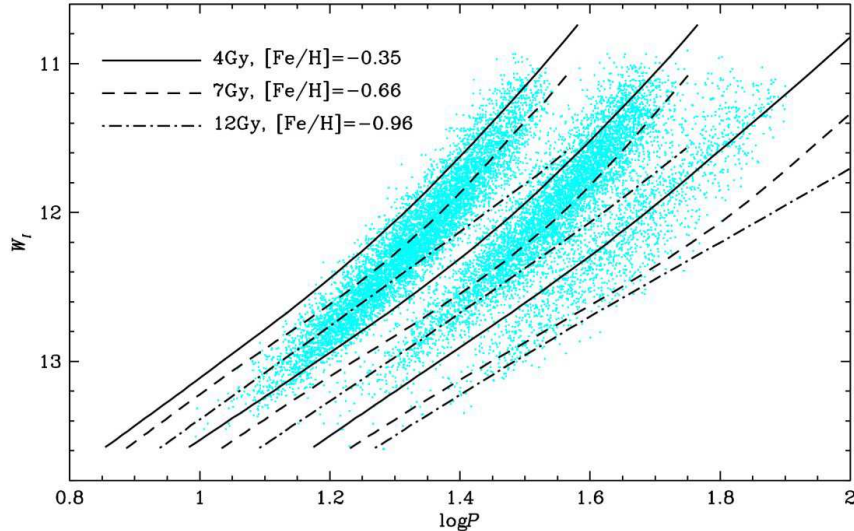


Fig. 7. Sequences  $b_1$ ,  $b_2$ , and  $b_3$  of the  $PL$  relation for the RGB OSARGs of the LMC (see Fig. 1) compared with relations calculated on the basis of the selected BaSTI isochrones for the first three radial modes. Ages and metal abundance parameters are given in legend. The initial masses in the order of increasing age are equal  $1.26 M_{\odot}$ ,  $1.02 M_{\odot}$ , and  $0.85 M_{\odot}$ . Mass loss in the RGB is included in the model calculations and the corresponding masses at the RGB-tip are  $1.13 M_{\odot}$ ,  $0.94 M_{\odot}$ , and  $0.79 M_{\odot}$ .

### 4.3 OSARGs as Solar-Like Pulsators

It is not yet known how pulsation observed in RGB and AGB stars are excited. Do they result from an intrinsic mode instability or rather, like in the sun, from a stochastic energy input to modes which are intrinsically stable. Both options have been considered Dziembowski *et al.* (2001) and by Bedding (2003). In both, there is a crucial role of convection which makes the problem difficult for theory. Phenomenological arguments, based on structure of power spectra, in favor for the solar-like option in the case of the SRVs were first given by Christensen-Dalsgaard *et al.* (2001) and supported by Bedding (2003). Power spectra of OSARGs resemble those of SRVs. Only the amplitudes are smaller. Thus, the solar-like option appears even more probable for OSARGs.

Stello *et al.* (2007) reported recently results of a multi-site search for solar-like oscillations in red giants in the open cluster M67. They did not report individual mode frequencies but only excess of power in some individual objects near location predicted by the scaling relation based on the solar data,

$$\nu_{\max} = \frac{(M/M_{\odot})(T_{\text{eff}}/T_{\text{eff}\odot})^{3.5}}{(L/L_{\odot})} \times 3050 \mu\text{Hz} \quad (3)$$

Bedding and Kjeldsen (2003) showed that this relation approximately describes location of the highest peaks in oscillation spectra of nearby dwarfs,



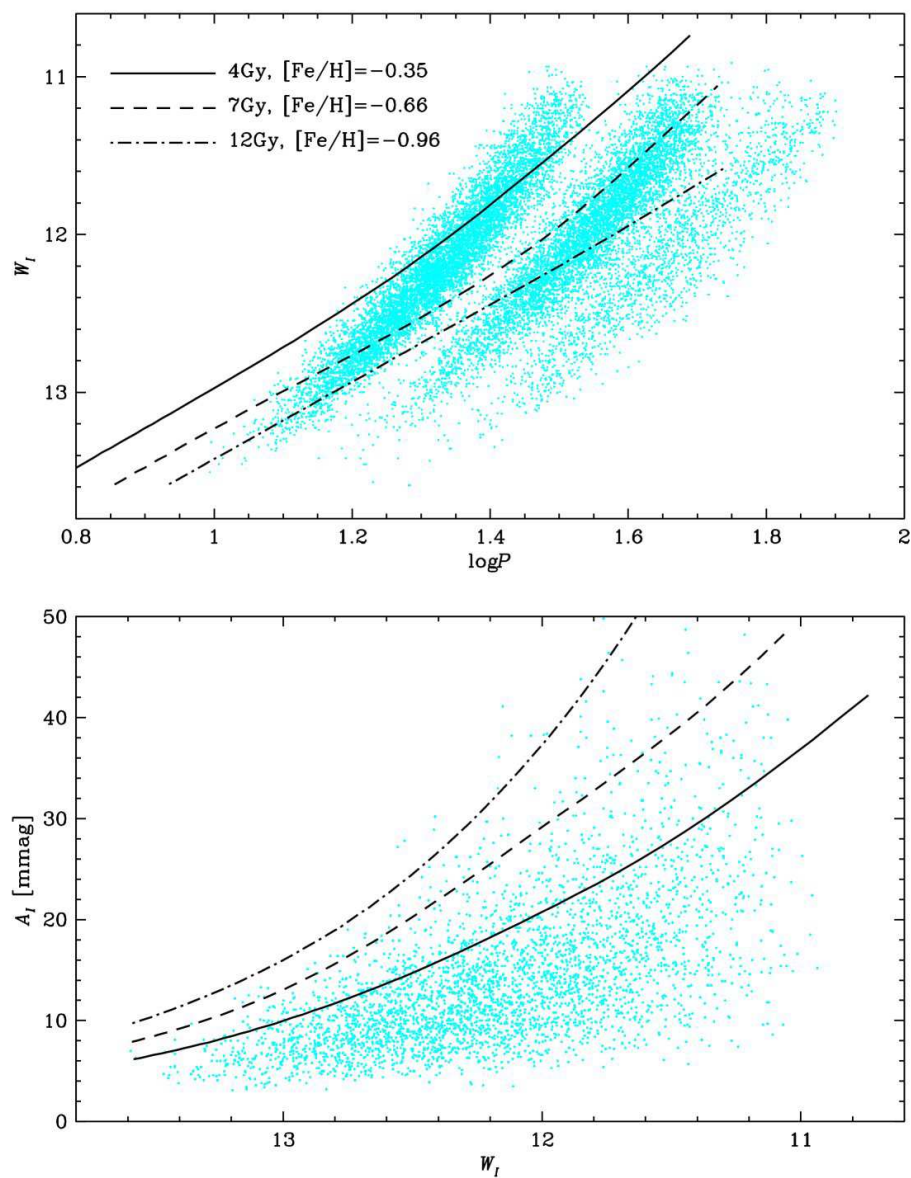


Fig. 8. The *upper panel* shows the same data as in Fig. 7 but the lines refer to periods ( $P_{\max} = \nu_{\max}^{-1}$ ) corresponding to maximum amplitude of solar-like oscillations calculated with Eq. (3) for the same isochrones as in Fig. 7. Dots in the *lower panel* shows the mode amplitudes for the RGB OSARGs of the LMC. The lines were calculated with Eq. (4) for the same isochrones as in the *upper panel*.



subgiants and giants. Stello *et al.* (2007) also compared the measured excesses of power with the scaling relation for peak amplitudes

$$A_\lambda = \frac{L/L_\odot(5.1 \pm 0.3) \mu\text{mag}}{(\lambda/550 \text{ nm})(T_{\text{eff}}/T_{\text{eff}\odot})^2(M/M_\odot)} \quad (4)$$

derived by Kjeldsen and Bedding (1995). Only for the objects lying in the lower RGB ( $L/L_\odot < 30$ ) they were able to find measurable excesses. The values are crudely consistent with the prediction. For brighter object they could derive only upper limits.

The RGB OSARGs are considerably brighter than the M67 red giants for which the excess have been measured. At  $W_I = 12$  mag their luminosity is between 1.5 and  $2 \times 10^3 L_\odot$ . How the two scaling relations work at these high luminosities is shown in Fig. 8. We used the same isochrones as adopted in the  $PL$  relations shown in the previous Section, to calculate  $P_{\text{max}} = 1/\nu_{\text{max}}$  using Eq. (3) and  $A_I$  using Eq. (4). In the latter, we adopted  $\lambda = 810$  nm.

In the upper plot we may see that maximum of power corresponds to the first and second overtone of radial modes. We may conclude that there is a crude agreement with data. At lower luminosity the calculated lines run well above the  $b_1$  sequence. However, we do not take it as an evidence against the solar-like interpretation of the OSARGs, because in all solar-like pulsators modes are seen in a rather wide range of frequencies. On the other hand, since in various stars low-order modes are excited by the other type of driving, even a very good agreement could not be regarded as a proof that the OSARGs are indeed solar-like pulsators.

As for the amplitude, the agreement is worse, as the lower panel of Fig. 8 shows. Again, the agreement should not be seen as evidence against the solar-like nature of the OSARGs. Eq. (4) is not based on any solid theory. In fact, a more recent study of stochastic excitation by Samadi *et al.* (2005) suggests the  $(L/M)^{0.7}$  amplitude scaling, instead of  $(L/M)$  adopted in Eq. (4). Slower amplitude rise is indeed more consistent with data. At this point, we just want to stress that the OSARGs are likely to provide the best constraints on models of stochastic excitation over a wide range of stellar parameters.

## 5. Miras and Semiregular Variables

Mira stars and SRVs are regarded as two different types of LPVs (Kholopov *et al.* 1985), although it seems that both groups represent a continuum. In the period–NIR luminosity diagrams these objects obey two parallel  $PL$  relations (sequences C and C') which are thought to represent fundamental and first overtone modes of pulsations. Soszyński *et al.* (2005) studied 3200 Miras and SRVs in the LMC and noticed important feature: in the period– $W_I$  diagram each  $PL$  sequence splits into two well separated ridges what corresponds to spectral division into O-rich and C-rich AGB stars.

In this paper we used the sample of Miras and SRVs in the LMC selected by Soszyński *et al.* (2005). We slightly corrected this list by applying the OSARG

indicator described in Section 4.1. This time we left on the list only variables with very small value of this parameter, smaller than 0.5. In the SMC we selected Miras and SRVs in the same manner as in the LMC and found in total 630 objects. From our fit we excluded stars redder than  $(J - K_S) = 2.3$  mag, *i.e.*, objects obscured by dust, and stars populating dim sequence between C and C' (see discussion below).

In our diagrams Miras and SRVs are indicated with pink (O-rich) and red (C-rich) points and lines. We plotted only one point per star corresponding to the most significant period. In the LMC the division into O- and C-rich variables was done in the period- $W_I$  diagram, where both populations can be easily distinguished. However, the most striking difference between  $PL$  relations of LPVs in the LMC and SMC again occurs in the period- $W_I$  plane. In the SMC O-rich and C-rich variables are much worse separated than in the LMC. Besides, there appears to be almost no bright O-rich Miras and SRVs in the SMC, what is a well known effect of lower metallicity. Therefore, in the SMC we used another widely used tool for distinguishing between O-rich and C-rich red giants -  $(J - K_S)$  colors. Stars bluer than  $(J - K_S) = 1.3$  mag have been recognized as O-rich giants, while the remaining objects as C-rich stars.

Let us focus on sequence C' occupied by probable first overtone SRVs. At the NIR domain this sequence is roughly parallel to OSARG  $PL$  relations, what was an argument for recognizing OSARGs as the same type of variables as Miras and SRVs, but pulsating in higher overtones (Wood *et al.* 1999). However, the same stars plotted in the  $\log P - W_I$  diagram reveal completely different behavior. The  $PL$  law of O-rich SRVs crosses the OSARG sequences, while C-rich variables are in different position relative to OSARGs. This discrepancy between NIR and optical  $PL$  diagrams suggests that OSARGs represent a different, presumably less evolved, population of stars than SRVs and Miras. To check this, we looked for OSARGs showing modes belonging to sequence C, which is defined by former types of variables.

Among 17 000 of stars in the LMC classified as OSARGs, we found only a few objects with distinct periodicity associated with sequence C. However, for these objects our classification as OSARGs is uncertain, because none of the secondary periods fall on sequence A, which belongs solely to OSARGs. It is probable that the OSARG signature in these stars is caused either by spurious periods or periods are real, but in fact associated with higher overtones of more evolved objects. In conclusion, we did not find any convincing examples of variables belonging to both classes: SRVs and OSARGs.

We noted that the secondary periods for some SRVs in both Clouds seem to follow an additional  $PL$  sequence located between sequences C and C'. Moreover, Soszyński *et al.* (2005) mentioned about a dim sequence located in the same place, but defined by the primary periods of some small amplitude SRVs (these stars are not shown in Figs. 1 and 3). If this sequence is real and corresponds to a radial mode, then sequence C cannot correspond to the fundamental mode. This would imply a revision of the mode identification in Miras and SRVs. In such a case one can expect that the fundamental-mode oscillations would be observed for periods by a factor of about two longer than those associated with

sequence C. Indeed, we have found a number of SRVs with secondary periods in this region of the PL diagram, *i.e.*, between sequences C and D. Unfortunately, binary systems (sequence E with halved periods) are also expected to populate this region, and we would not be able to distinguish between pulsation and ellipsoidal variations of SRVs in binary systems.

There is also a number of SRVs – mostly carbon stars – with secondary periods shorter than those from sequence C'. These periods could be associated with pulsation modes higher than the first overtone, however this problem needs further exploration.

We have already noted that the largest differences in the *PL* relations between the two Clouds are seen in the  $\log P$ – $W_I$  plane. This conclusion concerns especially O-rich stars which populate different range of magnitudes and the *PL* relations differ in slopes. The sequences in  $K_S$  and  $W_{JK}$  are more similar. In particular, the slopes of the *PL* relations are the same within the error limits in both environments. To derive the zero-point differences between *PL* laws, we assumed the same slope for the LMC and the SMC stars. For the whole sequence C and for O-rich sequence C', we obtained similar vertical distances of about 0.35 mag in  $K_S$  band and about 0.4 mag in  $W_{JK}$ . It is in agreement with the previously derived values: *e.g.*, 0.4 mag for dereddened  $K_0$  magnitudes obtained by Wood (1995) or 0.36 mag derived by Ita *et al.* (2004) for sequence C in  $K_S$  (not corrected for extinction). For carbon stars of sequence C' the zero-point difference is considerably larger, that is 0.43 mag in  $K_S$  and 0.47 mag in  $W_{JK}$ . Note that the last value is very close to the estimated difference between distance moduli of the LMC and SMC (*e.g.*, Udalski *et al.* 1999).

## 6. Long Secondary Periods

The longest period sequence in our *PL* pattern (sequence D) is associated with the most mysterious phenomenon connected with red giants variability. Long Secondary Periods (LSPs) represent the only unexplained type of large amplitude stellar variability known today. Wood *et al.* (2004) discussed possible explanations of the LSPs and concluded that most plausible mechanism that may cause LSPs is gravity mode excitation. However, recently Soszyński (2007) presented observational arguments for binary origin of the LSPs. In this scenario dust and gas originated in stellar wind form a cloud orbiting the red giant causing a periodic obscuration. Radial velocity measurements (Hinkle *et al.* 2003, Wood *et al.* 2004) are consistent with both low-mass companion and non-radial oscillations. However, our photometric data contain new hints supporting the former option.

Our samples of LSP variables were initially selected using their position in the  $\log P$ – $W_{JK}$  diagrams. After a visual inspection, we chose about 1600 LMC and 300 SMC distinct LSP stars with characteristic “eclipsing-like” light curves. The division into O-rich and C-rich stars in the LMC was based on the position in the  $\log P$ – $W_I$  diagram. For the SMC stars, just like in the case of Miras and SRVs, we relied only on the  $(J - K_S)$  colors.

The strong argument for a binary scenario is that the sequence D overlaps with sequence E, formed by red giants in binary systems, and seems to be a continuation of this ridge toward brighter stars (Soszyński *et al.* 2004b). It is striking that this behavior appears in all analyzed PL planes:  $\log P-K_S$  (Derekas *et al.* 2006),  $\log P-W_I$ ,  $\log P-W_{JK}$  for both Clouds. Moreover, we found that both sequences seem to match each other at other bandpasses:  $J$ ,  $I$  and even  $V$ . If the LSP phenomenon were caused by a stellar oscillation, it would have to be an unlikely coincidence.

In contrast to sequences C and C', the slopes of sequence D in the NIR domain are different in both galaxies. The LSP variables in the SMC define ridge of shallower slope than in the LMC. It is interesting that the same behavior exhibits sequence E defined by close binaries. We take this fact as another argument supporting binary explanation of the LSP phenomenon.

The name “long secondary periods” is somewhat misleading, because quite often amplitude of the LSP variability is higher than that associated with the short periods. Most of LSP stars are OSARGs both of RGB and AGB type. However, in the latter case the amplitudes are much higher. Thus our sample of objects showing LSP consist predominantly of the AGB OSARGs.

OSARG variables with the LSP modulation do not follow exactly the same  $PL$  relations as non-LSP stars. The larger LSP amplitudes, the larger discrepancy between  $PL$  sequences. Stars with the largest amplitudes of the LSP modulations have distinctly smaller mean luminosities compared to their non-LSP counterparts. Besides, there appears to be a correlation between the LSP amplitudes and the minimum periods of OSARG oscillations.

An interesting issue concerning LSPs is a relative number of red giants exhibiting this phenomenon. Typical values found in the literature are 25–30%. However, our examination shows that this proportion depends on the lower amplitude of the LSP variability concerned in analysis. Derekas *et al.* (2006) indicated that maximum possible amplitudes of the LSP modulation increase with luminosity of stars, but the smallest amplitudes are at the detection limit along the whole range of magnitudes. If the minimum detected amplitudes are around 10 mmag, than the LSPs appear for about 30% of LSPs. If the limit for amplitude is decreased to 5 mmag, the proportion of stars with LSPs reaches 50%. We can also consider the stars with LSP variations of amplitudes larger than pulsational (OSARG, SRV) amplitudes. Then, we detect the LSP modulation in about 30% of the whole sample.

Adopting the binary star scenario, we have to explain why the  $PL$  relation for the LSP is nearly parallel to  $PL$  relations for radial pulsation modes and why the phenomenon is so common. The near parallel run of the  $PL$  relations, translates to almost constant ratio of star to orbit radii,  $R/A$ . Combining the Kepler law with the expression for radial mode periods, we obtain

$$\frac{R}{A} = 0.24(1+q)^{-1/3} Q_k^{-2/3} \left( \frac{P_k}{P_{\text{orb}}} \right)^{2/3} \quad (5)$$

where  $q$ , which we will neglect, is the secondary companion to total mass ratio and  $Q_k$  is the pulsation constant. In Section 4.2, we associated the sequences  $b_k$

( $k=1,2,3$ ) of the  $PL$  relations for the RGB OSARGs with the first three radial modes and suggested the same association with sequences  $a_k$  ( $k=1,2,3$ ) for the AGB OSARGs. We follow it here and, in agreement with the adopted scenario, we set  $P_{\text{orb}} = P_{\text{LSP}}$ . The  $PL$  relation for LSP variables is defined primarily by the AGB OSARGs, thus we should use periods from the  $a_k$  sequences. Unfortunately, we do not have the  $Q_k$  values for the AGB star. However, we noted in our RGB star models that  $Q_2$  values change only little along the isochrones. In the considered models, the values rise from 0.024 to 0.025. We adopted the upper value and in the Petersen diagram identified the  $P_S/P_L = 0.05$  as the  $P_3/P_{\text{orb}}$  ratio. With these numbers, Eq. (5) yields  $R/A = 0.4$ .

What may keep the hypothetical low-mass companion in a narrow range of fractional distances away of stellar surface? Stars expand through the whole RGB and most of AGB phase. However, mass loss causes that orbits of their low-mass companions expand too. At typically adopted mass loss rates, the  $R/A$  ratio increases. As long as its value is well below one, tidal effects are negligible and changes of the orbital radius are determined only by mass loss from the star (we ignore here possible interactions with other companions). The rate of  $A$  decrease due to tidal friction is proportional to  $(R/A)^7$  (*e.g.*, Zahn 1977), so that once tidal effects become important, the sign of the temporal derivative of  $A$  may quickly reverse and it is usually assumed (*e.g.*, Villaver and Livio 2007) that the companion is engulfed into the red giant envelope. However, the tidal interaction affects also the star and it does not seem unreasonable to assume that it enhances mass loss. If the mass loss rate becomes sufficiently high the orbital distance may start to increase again and the companion migration toward the stellar surface may be halted. Stellar radius will then continue to increase but the  $R/A$  ratio will stay nearly constant at the value, which we estimated to be about 0.4.

Since about 30–50% of red giants exhibits the LSP variability and certainly there must be a range of unfavorable inclinations for its detection, we must postulate that nearly all red giants have their low mass companions. This would have far reaching consequences for our views on frequency planetary systems in the universe. We are aware of problems that the proposed scenario poses. However, the problems, with an alternative explanation of the LSP that postulates g-mode excitation seem even harder to overcome.

## 7. Ellipsoidal and Eclipsing Red Giants

The last class of LPVs represented in the rich structure of the  $PL$  distribution are red giants in the binary systems – ellipsoidal and eclipsing variables. Wood *et al.* (1999) suggested that sequence E is made up of contact binaries. It was confirmed by Ruciński and Maceroni (2001), who analyzed long-period eclipsing binaries detected in the OGLE SMC fields and indicated a distinct period–luminosity–color relation.

Soszyński *et al.* (2004b) selected and studied a sample of 1660 ellipsoidal and eclipsing binaries with a red giant as one of the components. They showed that

the scatter of the  $PL$  relation strongly depends on the amplitude of ellipsoidal variability – the larger amplitudes the tighter  $PL$  strip. It is understandable, because variables with the largest amplitudes must lay close to the line defined in the  $PL$  plane by systems with red giants filling up their Roche lobes. Obviously this theoretical line indicates the short period edge of the  $PL$  distribution, so the widening of the sequence must proceed toward longer periods.

Consequently, the determination of the  $PL$  relation depends on amplitudes of ellipsoidal variables – larger amplitude variables have on average shorter periods. To get consistent result in both galaxies, we cut the sample of Soszyński *et al.* (2004b) at  $A(I) = 0.03$  mag. We excluded also eclipsing variables, because eclipses of various depths randomly change the mean magnitudes of the stars. Finally, Soszyński *et al.* (2004b) showed that about 10% of ellipsoidal red giants reveal clear deformation caused by the eccentricity of their orbits. Periods of these systems are systematically longer than periods of ellipsoidal variables with circular orbits, therefore we removed the former group from our sample. In the SMC we selected ellipsoidal red giants in the same manner as in the LMC, and we found in total 440 objects.

Sequence E stars are marked in yellow in Figs. 1–5. Note, that in Wood *et al.* (1999) and in many subsequent papers this sequence was shifted toward shorter periods by a factor of two, because half the orbital periods were presented. The spread of sequence E in the NIR domain is considerably larger than in the period– $W_I$  plane. It can be partly explained by errors of the 2MASS photometry increasing quickly for fainter stars.

As it was noted in the previous Section, ellipsoidal variables in the LMC follow at NIR passbands somewhat steeper  $PL$  relation than in the SMC. Since the  $PL$  relation of ellipsoidal variables is a projection of radius–luminosity dependence, this fact can be utilized for studying parameters of red giant stars in environments of different metallicities.

## 8. Conclusions

In this paper we showed the most complex structure of the  $PL$  distribution presented so far. The Wood’s five ridges turn out to be an overlap of fourteen sequences (if consider closely spaced  $PL$  relations of OSARGs, the number of sequences exceeds twenty). In order to help recognizing  $PL$  relations with published  $PL$  laws we provide Table 3 with appropriate identifications.

Diagrams employing period ratios (similar to the Petersen diagram) were used as a tool for discriminating OGLE Small Amplitude Red Giants (OSARGs). We compared three sequences of the  $PL$  relations for the LMC OSARGs in the RGB phase with the calculated relation for first three radial modes using isochrone calculations. We found an essential agreement with our knowledge about metallicities and ages of red giants population in the LMC. However, there are also discrepancies which may suggest the necessity of refinement of the knowledge and/or stellar models. This is a potential application of the OSARGs.

T a b l e 3  
Labels of the  $PL$  relations in this and previous papers

| this paper    |                | Wood <i>et al.</i> 1999 | Kiss and Bedding 2003 | Ita <i>et al.</i> 2004 |
|---------------|----------------|-------------------------|-----------------------|------------------------|
|               | b <sub>1</sub> |                         |                       | $R_1$                  |
| RGB           | b <sub>2</sub> | B                       |                       | $R_2$                  |
|               | b <sub>3</sub> | A                       |                       | $R_3$                  |
| OSARGs        | a <sub>1</sub> |                         |                       |                        |
|               | a <sub>2</sub> | B                       |                       | 2O                     |
| AGB           | a <sub>3</sub> | A                       |                       | 3O                     |
|               | a <sub>4</sub> |                         |                       |                        |
| Miras         | O-rich         | C <sub>O</sub>          | C                     | F                      |
|               |                | C' <sub>O</sub>         | B                     | 1O                     |
| and SRVs      | C-rich         | C <sub>C</sub>          | C                     | F                      |
|               |                | C' <sub>C</sub>         | B                     | 1O                     |
| LSPs          | O-rich         | D <sub>O</sub>          | D                     | $L_2$                  |
|               | C-rich         | D <sub>C</sub>          | D                     | $L_2$                  |
| Ell. and Ecl. | E              | E*                      |                       | $L_1^*$                |

\* – the sequence is shifted due to halving the orbital periods.

Most likely mechanism responsible for pulsation in the OSARGs is the stochastic excitation. Therefore we looked at these objects as solar-like pulsators. The range of periods agrees with predictions based on extrapolation of the relations found for much less luminous stars. The amplitudes are lower than predicted by the Kjeldsen and Bedding (1995) formula, where the amplitude rises linearly with the luminosity-to-mass ratio. However, there are calculations predicting a slower amplitude rise. Testing theory of stochastic excitation is another possible application of OSARGs.

We would like to bring the reader's attention to NIR Wesenheit index ( $W_{JK}$ ). The sequences in the period- $W_{JK}$  plane are generally better defined than those at  $K_S$  magnitudes. Wesenheit index is a reddening independent quantity, so even heavily reddened Miras fall on the  $PL$  sequence. Therefore, the period- $W_{JK}$  relations can be used as distance indicators without correcting them for reddening. Moreover, O- and C-rich Miras and SRV obey very similar relations in the period- $W_{JK}$  plane, while at  $K_S$  the  $PL$  relations are significantly different for both populations. We conclude that  $W_{JK}$  index can be a useful tool for studying LPVs.

Comparison of the  $PL$  relations in NIR supports the binary star scenario as the explanation of the LSP variability. We further develop this scenario taking into account data on the ratios of the short period (pulsational) and LSP variability. For OSARGs this ratio is nearly constant which translates into nearly constant ratio of the stellar to orbital radius the value of about 0.4. We proposed that the small mass companion position is determined by the balance

between mass loss and tidal effects. This scenario requires that the proximity of the companion enhances mass loss. Moreover, it requires that a substantial fraction (majority) of red giants have such companions and that their mass cannot be too small.

**Acknowledgements.** The paper was supported by the Foundation for Polish Science through the Homing Program and by MNiSW grants: 1P03D01130 and N20303032/4275.

This publication makes use of data products from the Two Micron All Sky Survey, which is a joint project of the University of Massachusetts and the Infrared Processing and Analysis Center/California Institute of Technology, funded by the National Aeronautics and Space Administration and the National Science Foundation.

## REFERENCES

- Bedding, T. R. 2003, *Astrophys. and Space Sci.*, **284**, 61.  
 Bedding, T. R., and Kjeldsen, H. 2003, *Publ. Astron. Soc. Aust.*, **20**, 203.  
 Christensen-Dalsgaard, J., Kjeldsen, H., and Mattei, J.A. 2001, *Astrophys. J.*, **562**, 141.  
 Cioni, M.-R.L., Marquette, J.-B., Loup, C., Azzopardi, M., Habing, H.J., Lasserre, T., and Lesquoy, E. 2001, *Astron. Astrophys.*, **377**, 945.  
 Cioni, M.-R.L., *et al.* 2003, *Astron. Astrophys.*, **406**, 51.  
 Clayton, M.L., and Feast, M.W. 1969, *MNRAS*, **146**, 411.  
 Cutri, R.M., *et al.* 2003, “2MASS All-Sky Catalog of Point Sources”.  
 Drekas, A., Kiss, L.L., Bedding, T.R., Kjeldsen, H., Lah, P., and Szabó, G.M. 2006, *Astrophys. J. Letters*, **650**, L55.  
 Dziembowski, W.A., Gough, D.O., Houdek, G., and Sienkiewicz, R. 2001, *MNRAS*, **328**, 601.  
 Edmonds, P.D., and Gilliland, R.L. 1996, *Astrophys. J. Letters*, **464**, L157.  
 Eggen, O.J. 1977, *Astrophys. J.*, **213**, 767.  
 Feast, M.W., Glass, I.S., Whitelock, P.A., and Catchpole, R.M. 1989, *MNRAS*, **241**, 375.  
 Fraser, O.J., Hawley, S.L., Cook, K.H., and Keller, S.C. 2005, *Astron. J.*, **129**, 768.  
 Gerasimovič, B.P. 1928, *Proceedings of the National Academy of Science*, **14**, 963.  
 Glass, I.S., and Lloyd Evans, T. 1981, *Nature*, **291**, 303.  
 Groenewegen, M.A.T. 2004, *Astron. Astrophys.*, **425**, 595.  
 Henry, G.W., Fekel, F.C., Henry, S.M., and Hall, D.S. 2000, *Astrophys. J. Suppl. Ser.*, **130**, 201.  
 Hinkle, K.H., Lebzelter, T., Joyce, R.R., and Fekel, F.C. 2002, *Astron. J.*, **123**, 1002.  
 Hughes, S.M.G., and Wood, P.R. 1990, *Astron. J.*, **99**, 784.  
 Ita, Y., Tanabé, T., *et al.* 2004, *MNRAS*, **347**, 720.  
 Kholopov, P.N. *et al.* 1985, “General Catalog of Variable Stars”, The Fourth Edition, Nauka, Moscow.  
 Kiss, L.L., and Bedding, T.R. 2003, *MNRAS*, **343**, L79.  
 Kiss, L.L., and Bedding, T.R. 2004, *MNRAS*, **347**, L83.  
 Kjeldsen, H., and Bedding, T.R. 1995, *Astron. Astrophys.*, **293**, 87.  
 Lebzelter, T., Schultheis, M., and Melchior, A.L. 2002, *Astron. Astrophys.*, **393**, 573.  
 Madore, B.F. 1982, *Astrophys. J.*, **253**, 575.  
 Noda, S., *et al.* 2002, *MNRAS*, **330**, 137.  
 Osvalds, V., and Risley, A. M. 1961, *Publ. Leander McCormick Obs.*, **11**, 147.  
 Pietrinferni, A., Cassisi, S., Salaris, M., and Castelli, F. 2004, *Astrophys. J.*, **612**, 168.  
 Rucinski, S.M., and Maceroni, C. 2001, *Astron. J.*, **121**, 254.  
 Salaris, M., and Girardi, L. 2005, *MNRAS*, **357**, 669.



- Samadi, R., Goupil, M.-J., Alecian, E., Baudin, F., Georgobiani, D., Trampedach, R., Stein, R., and Nordlund, A. 2005, *Journal of Astrophysics and Astronomy*, **26**, 171.
- Soszyński, I., Udalski, A., Kubiak, M., Szymański, M., Pietrzyński, G., Żebruń, K., Szewczyk, O., and Wyrzykowski, L. 2004a, *Acta Astron.*, **54**, 129.
- Soszyński, I., Udalski, A., Kubiak, M., Szymański, M., Pietrzyński, G., Żebruń, K., Szewczyk, O., Wyrzykowski, L., and Dziembowski, W.A. 2004b, *Acta Astron.*, **54**, 347.
- Soszyński, I., Udalski, A., Kubiak, M., Szymański, M., Pietrzyński, G., Żebruń, K., Szewczyk, O., Wyrzykowski, L., and Ulaczyk, K. 2005, *Acta Astron.*, **55**, 331.
- Soszyński, I. 2007, *Astrophys. J.*, **660**, 1486.
- Stello, D., et al. 2007, *MNRAS*, **377**, 584.
- Udalski, A. 2003, *Acta Astron.*, **53**, 291.
- Udalski, A., Kubiak, M., and Szymański, M. 1997, *Acta Astron.*, **47**, 319.
- Udalski, A., Szymański, M., Kubiak, M., Pietrzyński, G., Soszyński, I., Woźniak, P., and Żebruń, K. 1999, *Acta Astron.*, **49**, 223.
- Udalski, A., Szymański, M., Kubiak, M., Pietrzyński, G., Soszyński, I., Woźniak, P., and Żebruń, K. 2000, *Acta Astron.*, **50**, 307.
- Villaver, E., and Livio, M. 2007, *Astrophys. J.*, **661**, 1192.
- Wilson, R.E., and Merrill, P.W. 1942, *Astrophys. J.*, **95**, 248.
- Wood, P. R. 1995, *IAU Colloq. 155: "Astrophysical Applications of Stellar Pulsation"*, **83**, 127.
- Wood, P.R. 2000, *Publ. Astron. Soc. Aust.*, **17**, 18.
- Wood, P.R., Olivier, E.A., and Kawaler, S.D. 2004, *Astrophys. J.*, **604**, 800.
- Wood, P.R., and Sebo, K.M. 1996, *MNRAS*, **282**, 958.
- Wood, P.R., et al. (MACHO team) 1999, in: *IAU Symp. 191*, "Asymptotic Giant Branch Stars", Ed. T. Le Bertre, A. Lébre, and C. Waelkens (San Francisco: ASP), 151.
- Zahn, J.-P. 1977, *Astron. Astrophys.*, **57**, 383.